Biosensors and Bioelectronics 131 (2019) 136–142

Contents lists available at ScienceDirect

Biosensors and Bioelectronics

journal homepage: www.elsevier.com/locate/bios

Ultrasensitive amyloid-β proteins detection based on curcumin conjugated ZnO nanoparticles quenching electrochemiluminescence behavior of luminol immobilized on Au@MoS_2/Bi_2S_3 nanorods

Xiaojian Li, Dan Wu, Hongmin Ma, Huan Wang, Yaoguang Wang, Dawei Fan, Bin Du, Qin Wei*, Nuo Zhang*

Key Laboratory of Interfacial Reaction & Sensing Analysis in Universities of Shandong, School of Chemistry and Chemical Engineering, University of Jinan, Jinan 250022, China

ARTICLE INFO

Keywords:
Curcumin conjugated ZnO nanoparticles
Amyloid-β proteins
ECL
Au functionalized MoS_2/Bi_2S_3 nanorods

ABSTRACT

This work reported curcumin quenched electrochemiluminescence (ECL) behavior of luminol with H_2O_2 as coreactant. To achieve excellent ECL signal, luminol was anchored on Au functionalized MoS_2/Bi_2S_3 nanorods (Luminol-Au@MoS_2/Bi_2S_3), which not only exhibited super catalysis for H_2O_2 decomposition to enhance the ECL intensity of luminol/H_2O_2 system, but also offered a satisfying substrate material for grafting more Au nanoparticles via Au-S binding which was used to adsorb luminol and primary antibodies. As an antioxidant, the hydrophobicity of curcumin limited its bioavailability. Herein, curcumin was conjugated with ZnO nanomaterials (ZnO-CR) to increase its dispersity in water which can make it more bioavailable. Moreover, the possible quenching mechanism between luminol/H_2O_2 system and ZnO-CR was ascribed to the consumption of superoxide radical ($O_2^{\bullet -}$) and energy transfer. The consumption amount of $O_2^{\bullet -}$ was calculated to be 1.2092 μM/mL through superoxide anion free radical detection kit. Besides, polydopamine was self-polymerized on the surface of ZnO-CR (PDA@ZnO-CR) to anchor secondary antibodies. In optimum parameter, the ECL immunosensor exhibited excellent performance for amyloid-β(Aβ) proteins detection with a wide detection range from 0.05 pg mL^{-1} to 10 ng mL^{-1} and a low detection limit of 21 fg mL^{-1} (S/N = 3).

1. Introduction

Curcumin, named flavonoid (1,7-bis(4-hydroxy-3-methoxyphenyl) -1,6-heptadiene-3,5-dione), has become a potential candidate for curing some diseases due to its astonishing anti-oxidant, anti-inflammatory, anti-carcinogenic, chemo-preventive, anti-angeogenic, anti-diabetic, anti-viral and antibacterial properties (Anand et al., 2008; Christian et al., 2010; Gangwar et al., 2013). And curcumin can be able to inhibit the activity of free radical species, which is mainly caused by the H atom from the C12 methylene group (Govindaraju et al., 2018; Hatcher et al., 2008). In the field of electrochemiluminescence (ECL) research, as a high efficiency luminescent reagent, luminol has been studied extensively. In order to obtain admirable ECL intensity, H_2O_2 is indispensable during the detecting process. Superoxide radical ($O_2^{\bullet -}$) which is produced by H_2O_2 and dissolved oxygen could react with luminol producing excited-state luminol for generating ECL signals (Jiang et al., 2017). As an anti-oxidant, curcumin exhibits free radical-scavenging activity (Patil et al., 2018) which can remove $O_2^{\bullet -}$ to induce the decrease of luminol behavior. Therefore, a sandwich immunosensor was developed based on curcumin quenching the ECL behavior of luminol. However, one of the greatest difficult problems in applying curcumin for bioanalysis is its low bioavailability which is caused by its hydrophobic nature. Recently, more attentions have focused on exploring the combination of curcumin and modern nanotechnology (Ahmed et al., 2012; Zhou et al., 2013). Nanoparticles (Tikekar et al., 2013), liposomes (S et al., 2011), micelles (Liu et al., 2013) and soy protein isolate (Tapal and Tiku, 2012) have been applied to improve the dispersibility and bioactivity of curcumin for clinical investigation (Pan et al., 2013). Curcumin doped ZnO nanomaterials (ZnO-CR) has been prepared through wet chemistry (Moussawi and Patra, 2016). Curcumin can act as an anti-oxidation agent to synthesize metal nanoparticles (El et al., 2015), nanorods (Moussawi and Patra, 2015) and metal complexes. Zn-curcumin complex is formed during the synthesized process of ZnO-CR (Khalil et al., 2013). To immobilize antibodies, polydopamine was self-polymerized on the surface of ZnO-CR (PDA@ZnO-CR). The quinone functional groups of PDA can form covalent

* Corresponding authors.
E-mail addresses: sdjndxwq@163.com (Q. Wei), zhangnuoujn@163.com (N. Zhang).

https://doi.org/10.1016/j.bios.2019.01.066
Received 25 November 2018; Received in revised form 14 January 2019; Accepted 30 January 2019
Available online 19 February 2019
0956-5663/

couple with amine-terminated biomolecules by Michael reactions (Wang et al., 2017).

To improve the sensitivity of quenching sandwich-type immunosensor, the substrate luminophore materials should hold efficient luminescence. Heterostructures materials between suitable transition metal sulfide semiconductors have lots of advantages, such as increasing spatial charge separation, facilitating electrical conductivity through band engineering, and exhibiting the synergistic effects between the two components, which make heterostructures materials holding more excellent electrochemical performances (Hong et al., 2014). MoS_2/Bi_2S_3 nanorods with excellent electrochemical performances can be prepared through hydrothermal method (Fang et al., 2017). It has been demonstrated that MoS_2 nanoflowers have good catalysis for decomposing H_2O_2 (Yin et al., 2016). In addition, MoS_2/Bi_2S_3 nanorods have lots of advantages, such as large specific surface area, favorable solubility and biocompatibility. Moreover, the S atoms of MoS_2/Bi_2S_3 nanorods provide many vacant orbitals to immobilize noble metal atoms (Au, Pd, Pt and so on) through coordinate bonds (Liu et al., 2016). In this work, Au functionalized MoS_2/Bi_2S_3 nanorods were utilized to immobilize luminol via covalent linkage between Au nanoparticles and the amino- of luminol (Luminol-Au@MoS_2/Bi_2S_3). Combining the merits of MoS_2/Bi_2S_3 nanorods, Luminol-Au@MoS_2/Bi_2S_3 exhibited high luminous intensity, which had great potential applications in bioanalysis.

Alzheimer's disease (AD) as one of neurodegenerative disorders, will lead to losing and changing of memory, cognitive ability and even personality. Thus, AD will threaten human health and decrease life quality seriously (Shankar et al., 2007). It has been demonstrated that depositing of Amyloid-β (Aβ) proteins is related to the pathogenesis of AD (Yu et al., 2014). Aβ-42 and Aβ-40 are the two predominant forms of Aβ proteins (Triguero et al., 2008). Aβ-42, which is more hydrophobic and easily to aggregate than Aβ-40, is the major ingredient in the plaques of AD individuals (Vestergaard et al., 2005). In this work, Aβ-42 was utilized as a protein model to fabricate ECL immunosensor and polyclonal antibody was produced by immunizing animals with a synthetic peptide of β-amyloid. Therefore, the quantification of Aβ proteins during early stages of AD progress is extremely important (Selkoe, 2001). Herein, a sandwich ECL immunosensor with PDA@ZnO-CR quenching the ECL behavior of luminol/H_2O_2 system was fabricated. As shown in Scheme 1, primary antibodies (Ab_1) were anchored on Luminol-Au@MoS_2/Bi_2S_3 through Au adsorbing proteins. After secondary antibodies (Ab_2) labeled on PDA@ZnO-CR incubated on the modified electrode, the ECL behavior of luminol decreased obviously in the presence of H_2O_2. This may be due to the consumption of $O_2^{\bullet -}$ and energy transfer between curcumin and luminol/H_2O_2 system.

2. Experimental section

2.1. Preparation of luminol-Au@MoS_2/Bi_2S_3

MoS_2/Bi_2S_3 nanorods and Au@MoS_2/Bi_2S_3 nanorods were prepared according to the literature (Fang et al., 2017) and the detailed step was put in Supplementary materials. Au@MoS_2/Bi_2S_3 nanorods were redispersed in 5 mL ultrapure water. Then, 1 mL 5 mM luminol (pH 7.4) was mixed with the above solution under oscillating 12 h. Luminol was combined with Au@MoS_2/Bi_2S_3 nanorods via covalent linkage between Au nanoparticles and the amino- of luminol, centrifuging to remove dissociative luminol. Finally, the nanomaterials were vacuum drying at 35 °C. The obtained Luminol-Au@MoS_2/Bi_2S_3 nanomaterials were dispersed in 0.5% chitosan.

2.2. Synthetization of Ab_2-PDA@ZnO-CR

ZnO-CR was prepared according to the literature with small modifications (Moussawi and Patra, 2016). 5.0 mg curcumin was dispersed in 50 mL ultrapure water and then refluxed at 90 °C until curcumin dissolved. Then, 50 mL 0.1 M $Zn(NO_3)_2$ was mixed with above solution and refluxed for 1 h at 90 °C. When the solution was cooled down, 5 mL 0.2 M KOH was added dropwise at 4 °C. Following that, an orange yellow gel-like suspension was viewed, centrifuging 8000 rpm and washing with ultrapure water and acetone respectively at last time to remove unbound curcumin. The precipitate ZnO-CR was vacuum dried at 35 °C.

20 mg ZnO-CR and 1.5 mg dopamine were dissolved in 30 mL ultrapure water with stirring 6 h. Then, the mixed solution was centrifuged to remove unbonded dopamine. 10 mL 10 mM Tris-HCl (pH 8.5) was added under stirring 12 h, following that centrifuging at 8000 rpm and washing with water five times to remove unbound PDA. The obtained PDA@ZnO-CR was dried at 30 °C in vacuum. Then PDA@ZnO-CR was redispersed in 5 mL PBS (pH 7.4) and 500 μL 500 μg mL^{-1} Ab_2 was mixed with the solution with stirring 6 h at 4 °C. Finally, the above solution was mixed with 100 μL 1% BSA which can confine the

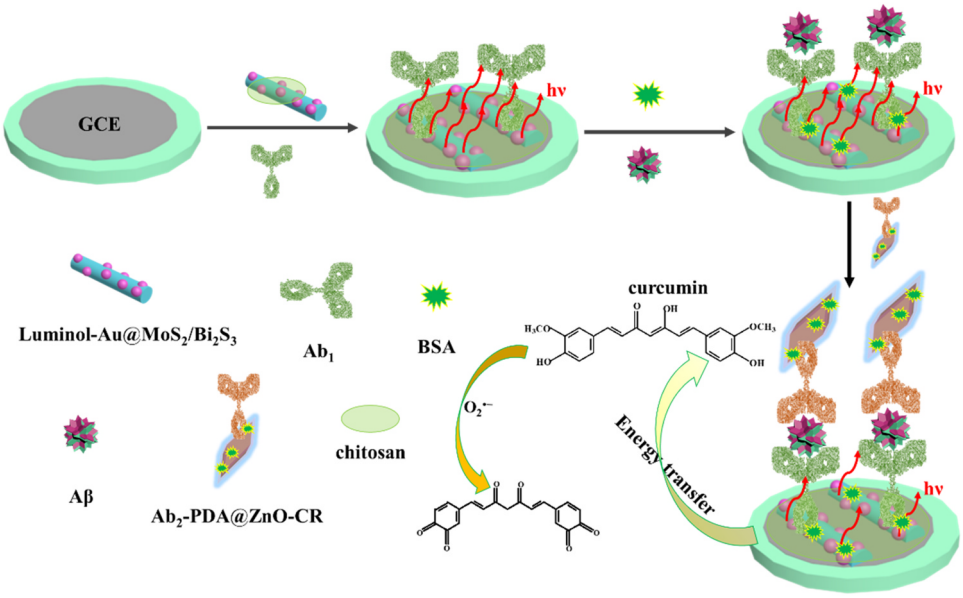

Scheme 1. Schematic representation of the fabrication of immunosensor.

nonspecific sites, followed by centrifuging and washing with ultrapure water to remove unbound BSA. The resulting Ab_2-PDA@ZnO-CR was dispersed in PBS (pH 7.4) and stored at 4 °C until use.

2.3. Immunoassay development for detecting Aβ proteins

The fabricated process of immunosensor was exhibited in Scheme 1. Before dropping nanomaterials and biomolecules, glassy carbon electrode (GCE) was pretreated by alumina slurries obtaining a mirror-like surface, then washed with ultrapure water. Subsequently, 7 μL 10 mg mL^{-1} Luminol-Au@MoS_2/Bi_2S_3 were modified on the GCE surface. Then, 6 μL Ab_1 (500 μg mL^{-1}) was incubated with the modified electrode surface at 4 °C for at least 2 h. After that, the modified-GCE was rinsed completely with ultrapure water and 3 μL 1 wt% BSA solution was modified on the GCE surface to block nonspecific sites for 1 h at 4 °C. Then the modified-electrode was rinsed with ultrapure water. Following that, 6 μL Aβ proteins solutions with different concentrations were incubated at 4 °C for 3 h. At last, Ab_2-PDA@ZnO-CR solution was combined with Aβ proteins/BSA/Ab_1/Luminol-Au@MoS_2/Bi_2S_3 modified GCE through immunoreaction between antibodies and antigens. The resulting immunosensor (Ab_2-PDA@ZnO-CR/Aβ proteins/BSA/Ab_1/Luminol-Au@MoS_2/Bi_2S_3/GCE) was stored at 4 °C until use.

2.4. ECL measurement

The substrate solution in ECL cell contained 10 mL PBS (pH 8.0) with 5 mM H_2O_2. The working potential was −0.2 to 0.6 V and the photomultiplier tube (PMT) was set at 600 V. The scan rate was set at 0.15 V s^{-1}. Then the resulting immunosensor was put in the ECL cell and investigated the ECL performance.

3. Results and discussion

3.1. Materials characterization

As illustrated in Fig. 1A, MoS_2/Bi_2S_3 nanorods with a mean diameter of 100 nm could be clearly observed. Fig. S1A was the energy dispersive X-Ray spectroscopy (EDX) of MoS_2/Bi_2S_3 nanorods which indicated the main elements of MoS_2/Bi_2S_3 nanorods including Mo, S and Bi. Fig. 1B showed the morphology of Au@MoS_2/Bi_2S_3 nanorods which demonstrated that Au nanoparticles were immobilized on MoS_2/Bi_2S_3 nanorods surface through Au-S chemical bond. Moreover, the EDX (Fig. 1C) and high-resolution transmission electron microscopy (HRTEM, Fig. 1D) of Au@MoS_2/Bi_2S_3 nanorods could also demonstrate that Au@MoS_2/Bi_2S_3 nanorods were successfully synthesized. HRTEM energy dispersive X-ray analysis (EDAX) mapping resulted the location of little Mo (Fig. S1-B1) which was distributed on the surface of MoS_2/Bi_2S_3 nanorods in consistent with the HRTEM imagines of Au@MoS_2/Bi_2S_3 nanorods, Au (Fig. S1-B2), Bi (Fig. S1-B3) and S (Fig. S1-B4), respectively. The lattice distance of Au nanoparticles and MoS_2/Bi_2S_3 nanorods (Fig. S2) was found to be 0.202 nm and 0.427 nm respectively with a high crystallinity. X-ray diffraction (XRD) characterization was conducted to further study the structure of the synthesized MoS_2/Bi_2S_3 nanorods. Fig. S3A was the XRD characterization of MoS_2/Bi_2S_3 nanorods, indicating that the characteristic diffraction peaks of which was assigned to Bi_2S_3. The XRD result was compared with the standard diffraction data of Bi_2S_3 (JCPDS card No. 17–0320). However, the characteristic diffraction peaks of MoS_2 were not observed in the XRD pattern of MoS_2/Bi_2S_3 nanorods. This may be due to MoS_2 occupied lower content in MoS_2/Bi_2S_3 nanorods resulting in the relatively weak diffraction intensity contrasting with Bi_2S_3 in MoS_2/Bi_2S_3 nanorods (Fang et al., 2014).

SEM image of ZnO-CR was presented in Fig. 1E and the particles looked like grain or half grain with mean sizes ranged from 200 to 350 nm width and 450–1000 nm length. The possible chelation mechanism of reaction between Zn^{2+} and curcumin was proposed in Fig. S4 and the detailed description was showed in Supplementary materials. The XRD pattern of ZnO-CR was characterized in Fig. S3B. All the diffraction peaks of ZnO-CR can be assigned to the Zincite ZnO (JCPDS No. 36–1451). Diffraction peaks were observed at 31.8° (100), 34.4° (002), 36.3° (101), 47.5° (102), 56.6° (110) and 62.9° (103), 68.0° (112) and 69.1° (201) with cell parameters a:3.250 Å, b:3.250 Å and c:5.207 Å. The additional peak found at 59.72° were attributed to curcumin (Moussawi and Patra, 2016). Compared with the pure ZnO-CR, PDA film was observed on the surface of PDA@ZnO-CR (Fig. 1F). Besides, Fourier transform infrared (FT-IR) spectrum can prove the existence of PDA. Fig. S5A curve a exhibited the FT-IR spectrum of curcumin. The peak at 1624 cm^{-1} as a mainly mixed ν(C=C) and ν(C=O) stretching vibration. The stretching vibration band at 1510 cm^{-1} in the curcumin FT-IR spectrum was belonged to mainly mixed vibrations of ν(C=O), δ(CC=O), and δ(CCC) (Kolev et al., 2005). After curcumin conjugated ZnO, the peak at 1650 cm^{-1} could be ascribed to ν(C=O) of curcumin (curve b). FT-IR spectra (curve c) depicted that characteristic peaks of PDA, identified with C=C and C-N at 1630 cm^{-1} and 1400 cm^{-1}, respectively (Chen et al., 2015). Compared PDA with PDA@ZnO-CR (curve d), the characteristic peak was consistent, indicating that ZnO-CR was capped by PDA. The optical properties of curcumin and ZnO-CR were investigated by fluorescence emission spectra (FL) (Fig. S5B) and UV–vis absorbance spectra (Fig. S5D). Fig. S5B illustrated the FL spectrum of curcumin (curve a), it can be seen that curcumin in aqueous solution possessed maximal emission at 560 nm and the excitation wavelength was at 400 nm. When curcumin conjugated ZnO, the maximal emission of ZnO-CR was shifted to 600 nm under the same conditions (curve b). As shown in Fig. S5D, the characteristic absorbance peak of curcumin was located at 362 nm (curve a). After curcumin conjugated ZnO, the characteristic absorbance peak produced red shift to 406 nm (curve b). And PDA caused the characteristic absorbance peak of ZnO-CR red shift to 510 nm (curve c). However, PDA exhibited no characteristic absorbance peak (curve d).

Cyclic voltammetry (CV) of MoS_2/Bi_2S_3 nanorods, luminol, Luminol-Au@MoS_2/Bi_2S_3, ZnO-CR and ZnO-CR/Luminol-Au@MoS_2/Bi_2S_3 was conducted in PBS (pH = 8.0) without (Fig. 2A) or with (Fig. 2B) H_2O_2. As shown in Fig. 2A, CV behavior of bare GCE exhibited no obvious peak (curve a). After MoS_2/Bi_2S_3 nanorods modified-electrode, the oxidative peak potential was at 0.077 V and a little reductive peak was observed at −0.17 V (curve b). When luminol added in the substrate solution, a redox couple (curve c) was displayed at 0.39 V (oxidative peak) and 0.075 V (reductive peak). Curve d showed the CV performance of Luminol-Au@MoS_2/Bi_2S_3 and the oxidative peak and reductive peak potential shifted to 0.644 V and 0.37 V, respectively, ascribed to the addition of Au and luminol nanoparticles. After ZnO-CR immobilized on the Luminol-Au@MoS_2/Bi_2S_3 modified-electrode, the oxidative peak and reductive peak potential remained unchanged, but the current intensity slightly increased (curve e). Besides, the electrochemical performance of ZnO-CR was investigated in Fig. S5C curve a and the oxidative peak and reductive peak potential was located at 0.12 V and 0.02 V, respectively. Analogous to catechol groups forming quinone molecules function (Kim et al., 2014; Liu et al., 2007), curcumin can act as a redox shuttle for the transfer of protons and electrons (eq. 6). Fig. 2B curve a was the CV of bare GCE and when Au@MoS_2/Bi_2S_3 was immobilized on the electrode surface, the current from 0.8 to 1.0 V increased (Fig. 2B, curve b), indicating Au@MoS_2/Bi_2S_3 can catalyze the decomposition of H_2O_2. However, when the substrate solution containing H_2O_2, the oxidative peak of Luminol-Au@MoS_2/Bi_2S_3 (Fig. 2B, curve c), and luminol (Fig. 2B, curve e) was disappeared due to luminol reacted with H_2O_2. As shown in Fig. S5C curve b, the oxidative peak of ZnO-CR at 0.12 V was also disappeared, indicating that curcumin as an antioxidant can react with and $O_2^{\bullet-}$ generating electro-oxidation products of curcumin (eq. 7). This process may lead the disappearance of oxidative peak. But, when ZnO-CR and Luminol-Au@MoS_2/Bi_2S_3 co-existed on the electrode surface (Fig. 2B, curve d), the oxidative peak of Luminol-Au@MoS_2/Bi_2S_3 still existed, but the current

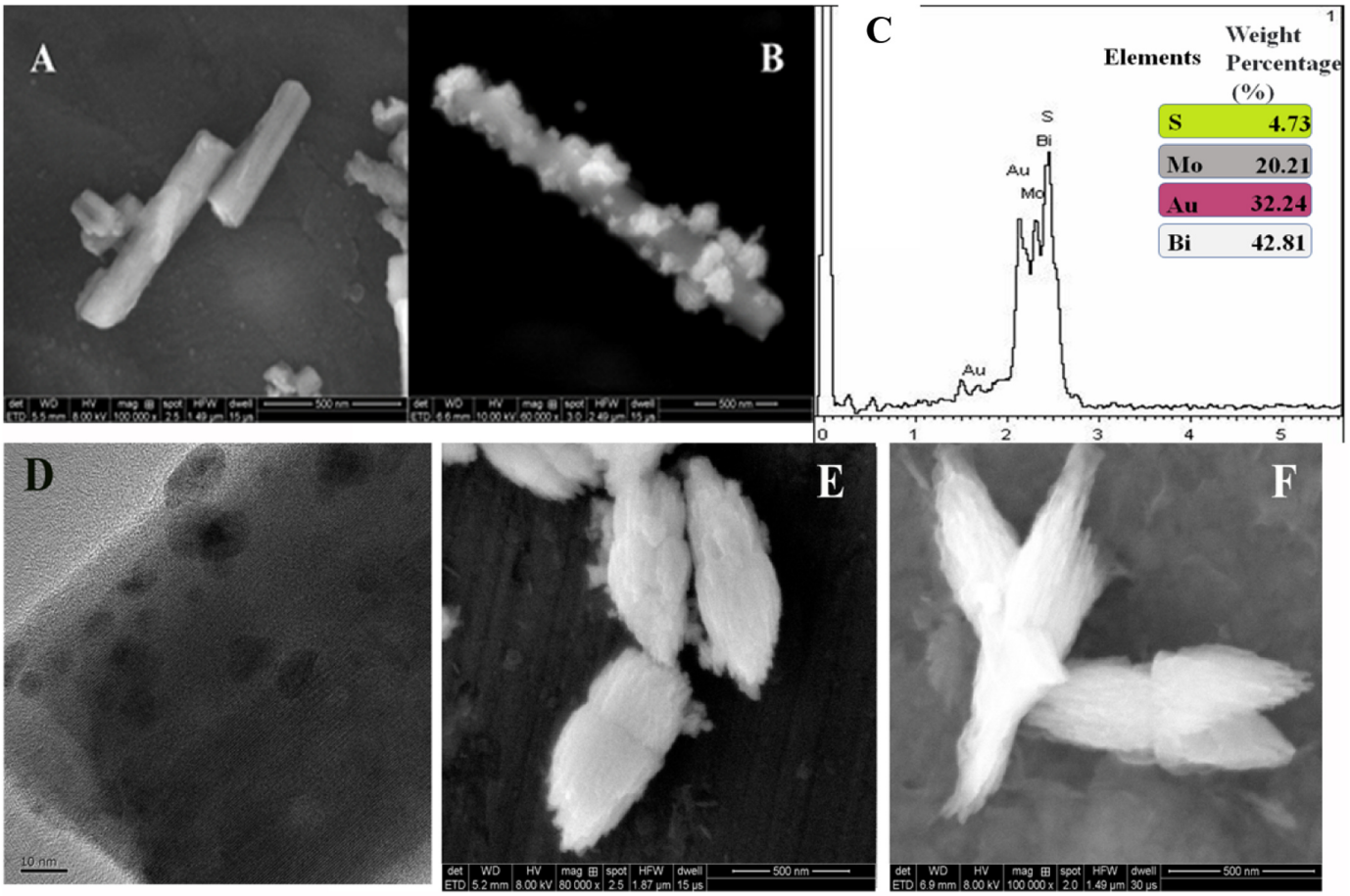

Fig. 1. SEM imagines of MoS_2/Bi_2S_3 (A), Au@MoS_2/Bi_2S_3 (B), ZnO-CR (E) and PDA@ZnO-CR (F); EDX (C) and HRTEM (D) of Au@MoS_2/Bi_2S_3 nanorods.

intensity decreased. This may be due to there being competition reaction between curcumin and luminol with $O_2^{\bullet -}$ produced by H_2O_2. Thus, curcumin showed more effective scavenging activity towards free radical species and curcumin can become ECL quencher to annihilate the ECL behavior of luminol/H_2O_2 system.

3.2. ECL mechanism of luminol-Au@$MoS_2/Bi_2S_3/H_2O_2$ system and ZnO-CR quenching luminol-Au@MoS_2/Bi_2S_3 nanorods

In this work, Au@MoS_2/Bi_2S_3 nanorods efficiently catalyzed H_2O_2 to superoxide anion $O_2^{\bullet -}$ (eq. 1)·H_2O_2 was used as coreactant to react with luminophore luminol generating ECL behavior. Luminol molecules can lose a hydrogen ion forming luminol anion (Lu^-) in alkaline electrolyte, then a positive potential sweep makes Lu^- generate luminol radical anion $Lu^{-\bullet}$ (eq. 2). Subsequently, $Lu^{-\bullet}$ reacts with $O_2^{\bullet}$ formed excited state 3-aminophthalate (3-AP^{2-*}) and N_2 (eq. 3). Moreover, $O_2^{\bullet}$ can react with Lu^- producing $Lu^{-\bullet}$ and HO_2^- which can further lose electron to form $O_2^{\bullet}$ (eq. 4). When excited state 3-AP^{2-*} bank to ground state 3-AP^{2-}, strong luminescence emission at 425 nm is observed (eq. 5) (Yang et al., 2018). Obviously, ECL signals of luminol are directly in proportion to the

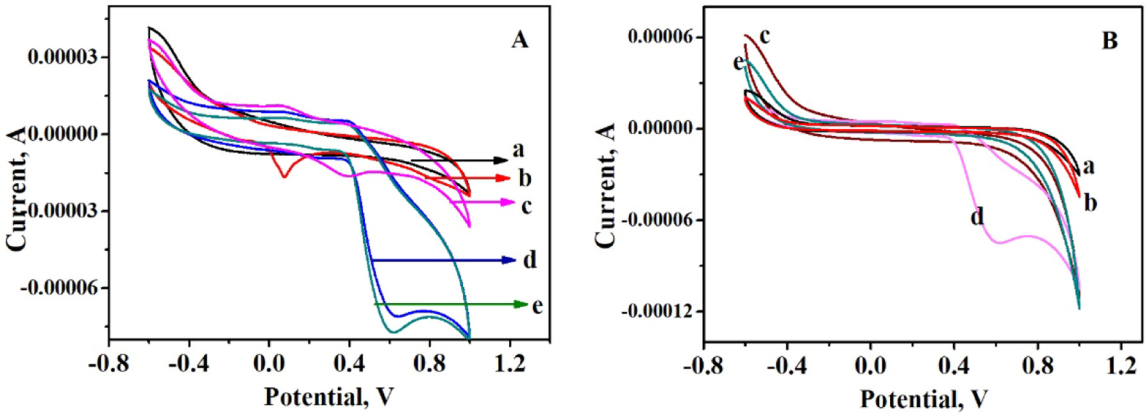

Fig. 2. (A) CV of bare GCE (a), MoS_2/Bi_2S_3 nanorods/GCE (b), luminol/GCE (c), Luminol-Au@MoS_2/Bi_2S_3/GCE (d) and ZnO-CR/Luminol-Au@MoS_2/Bi_2S_3/GCE (e) performed in PBS (pH = 8.0) without H_2O_2. (B) CV of bare GCE (a), Au@MoS_2/Bi_2S_3/GCE (b), Luminol-Au@MoS_2/Bi_2S_3/GCE (c), ZnO-CR/Luminol-Au@MoS_2/Bi_2S_3/GCE (d) and luminol/GCE (e) performed in PBS (pH = 8.0) with 5 mM H_2O_2.

concentration of $O_2^{\bullet -}$, which is determined by the concentration of H_2O_2. As an antioxidant, curcumin exhibits free radical-scavenging activity which can remove $O_2^{\bullet -}$ and the oxidation product was speculated based on the research of Aleksander Ciszewski (eq. 7) (Ciszewski et al., 2003; Patil et al., 2018). To prove the amount of $O_2^{\bullet -}$ decreased, superoxide anion free radical detection kit was used to detect the amount of $O_2^{\bullet -}$. The detailed detecting process was shown in Supplementary materials. As shown in Fig. S6, a linear relationship between the concentration of NO_2^- and absorbance at 530 nm was obtained. Fig. S7A was the substrate solution of Luminol-Au@MoS_2/Bi_2S_3/GCE and the reddish solution was exhibited. However, when the electrode was modified with Ab_2-PDA@ZnO-CR/Aβ/BSA/Ab_1/Luminol-Au@MoS_2/Bi_2S_3/GCE, color is almost invisible (Fig. S7B). Using that data, the concentration of $O_2^{\bullet -}$ without and with Ab_2-PDA@ZnO-CR was 1.382 μM/mL and 0.1728 μM/mL, respectively. Based on this, the ECL behavior of luminol/H_2O_2 system should be quenched by curcumin. To further investigate the detail mechanism of curcumin quenching luminol ECL principle, FL experiments were conducted.

The FL spectrum of luminol exhibited maximum emission at 440 nm and the excitation wavelength was at 400 nm (Fig. 3A, curve a). Obviously, the FL emission at 440 nm was annihilated after the introduction of curcumin, ZnO-CR and PDA@ZnO-CR successively with the same concentration and this may be due to the hydrophobic of curcumin. This quenching behavior can be occurred due to the overlap between the absorption spectra of curcumin (400–600 nm) and the emission spectra of luminol (420–580 nm). Meanwhile, as shown in Fig. 3B, the consisted ECL behavior of Luminol-Au@MoS_2/Bi_2S_3/GCE (a), curcumin/Luminol-Au@MoS_2/Bi_2S_3/GCE (b), ZnO-CR/Luminol-Au@MoS_2/Bi_2S_3/GCE (c) and PDA@ZnO-CR/Luminol-Au@MoS_2/Bi_2S_3/GCE (d) with the same concentration in PBS (pH = 8.0) with 5 mM H_2O_2 was performed. Contrary to FL results, curcumin which dissolved in absolute ethyl alcohol can be more effectively quenched the ECL behavior of luminol than ZnO-CR due to a higher amount of curcumin. But, compared with ZnO-CR, the same concentration of PDA@ZnO-CR exhibited around the same ECL quenching efficiency toward Luminol-Au@MoS_2/Bi_2S_3 modified-electrode. Thus, not only the energy transfer but also the consumption of free radical species that was a reactant to react with curcumin, quenched the ECL emission of luminol.

3.3. Characterizations of proposed ECL immunosensor

In order to characterize the fabrication process of the proposed ECL immunosensor, electrochemical impedance spectroscopy (EIS) characterizations of each step were conducted in 2.5 mM $K_3Fe(CN)_6$/$K_4Fe(CN)_6$ and 0.1 M KNO_3 solution. EIS characterizations were simulated through ZSimpWin software (solid line was the fitting curve) in Fig. 3C and the inset was the equivalent circuit for EIS, which contained four elements: the ohmic resistance of the electrolyte solution (R_s); electron-transfer resistance (R_{et}); Constant phase element (Q) and Warburg impedance (Zw). Fig. 3C showed that Ret of Luminol-Au@MoS_2/Bi_2S_3 (curve b) was larger than bare GCE (curve a). After Ab_1, BSA and Ab_2-PDA@ZnO-CR on the modified electrode, the semicircle domains were successively increased (curves c-e, respectively). This result can be ascribed to that the formed protein layer acting as non-electroactive molecules, obviously restrained the diffusion of

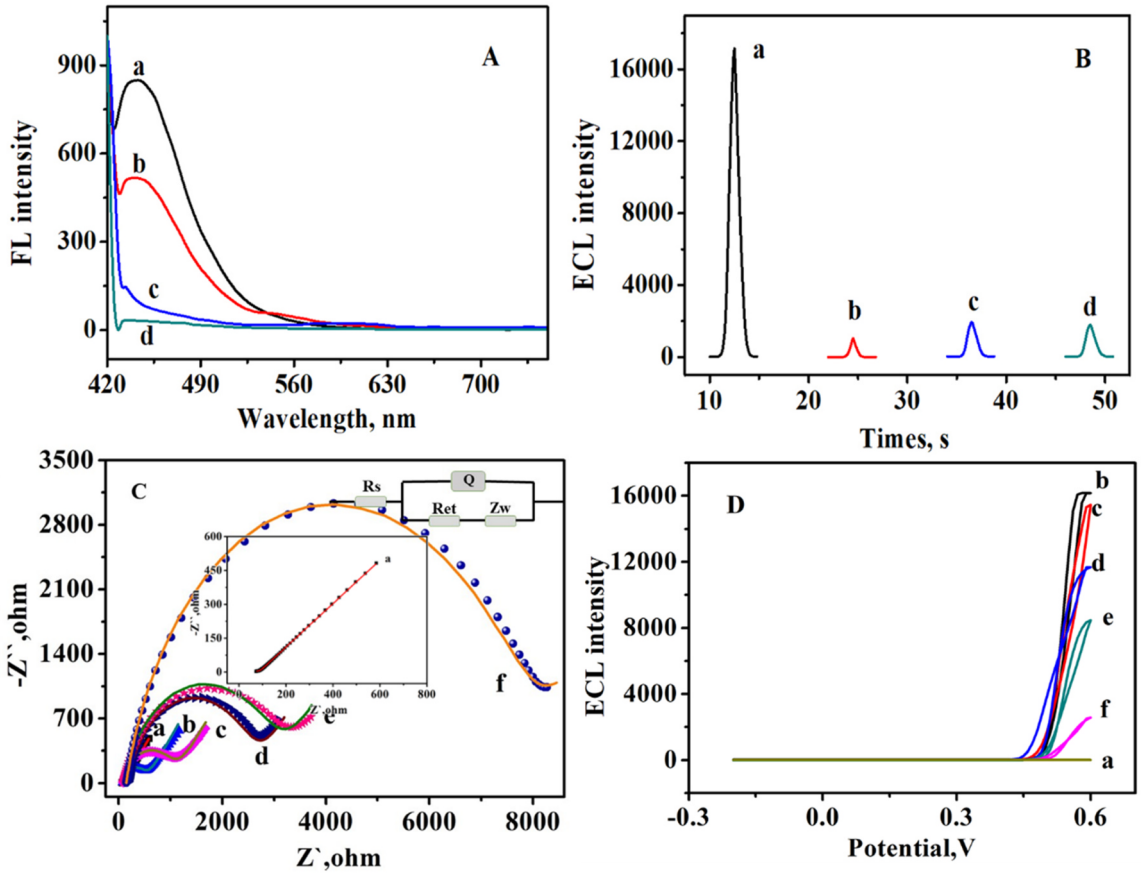

Fig. 3. (A) FL spectra of luminol (a), curcumin-luminol (b), ZnO-CR-luminol (c), and PDA@ZnO-CR-luminol (d); (B) The ECL behavior of Luminol-Au@MoS_2/Bi_2S_3/GCE (a), curcumin/Luminol-Au@MoS_2/Bi_2S_3/GCE (b), ZnO-CR/Luminol-Au@MoS_2/Bi_2S_3/GCE (c) and PDA@ZnO-CR/Luminol-Au@MoS_2/Bi_2S_3/GCE (d) in PBS (pH = 8.0) with 5 mM H_2O_2; (C) The EIS and fitting curves of bare GCE (a), Luminol-Au@MoS_2/Bi_2S_3/GCE (b), Ab_1/Luminol-Au@MoS_2/Bi_2S_3/GCE (c), BSA/Ab_1/Luminol-Au@MoS_2/Bi_2S_3/GCE (d), Aβ/BSA/Ab_1/Luminol-Au@MoS_2/Bi_2S_3/GCE (e) and Ab_2-PDA@ZnO-CR/Aβ/BSA/Ab_1/Luminol-Au@MoS_2/Bi_2S_3/GCE (f) performed in 2.5 mM $Fe(CN)_6^{3-/4-}$ and 0.1 M KNO_3; The insets are the equivalent circuit for EIS and EIS spectra of bare GCE (a); (D) The ECL profiles of bare GCE (a), Luminol-Au@MoS_2/Bi_2S_3/GCE (b), Ab_1/Luminol-Au@MoS_2/Bi_2S_3/GCE (c), BSA/Ab_1/Luminol-Au@MoS_2/Bi_2S_3/GCE (d), Aβ/BSA/Ab_1/Luminol-Au@MoS_2/Bi_2S_3/GCE (e) and Ab_2-PDA@ZnO-CR/Aβ/BSA/Ab_1/Luminol-Au@MoS_2/Bi_2S_3/GCE (f) performed in PBS (pH = 8.0) containing 5 mM H_2O_2.

ferricyanide and hindered electron transfer between ferricyanide and the electrode surface (Han et al., 2017; Li et al., 2017). Table S1 exhibited the corresponding fitting data and Ret value which represented the degree of modified electrode surface towards electron mediator. The Ret value increased after successively incubation of Luminol-Au@MoS_2/Bi_2S_3, Ab_1, BSA, Aβ proteins, and Ab_2-PDA@ZnO-CR, in agreement with the semicircle domains of EIS. These results indicated that the ECL immunosensor was successfully fabricated.

To further confirm the modified-electrodes fabrication process, the corresponding ECL-potential profiles were performed in PBS (pH 8.0) including 5 mM H_2O_2 and exhibited in Fig. 3D. When Luminol-Au@MoS_2/Bi_2S_3 modified on the electrode surface (curve b), an obvious ECL signal was exhibited (curve a). After successive modification with Ab_1 (curve c), BSA (curve d) and Aβ proteins (curve e), the ECL intensity decreased, respectively. This may be due to the insulation effect of Ab_1, BSA and Aβ proteins which hindered the electron-transfer between luminol and coreactant H_2O_2. Finally, the ECL intensity was significantly decreased after incubating with Ab_2-PDA@ZnO-CR (curve f). The dramatically change could be ascribed to ZnO-CR effectively quenching the ECL of Luminol-Au@MoS_2/Bi_2S_3.

3.4. Detecting Aβ proteins by the fabricated ECL immunosensor

To obtain unexceptionable ECL behavior of Luminol-Au@MoS_2/Bi_2S_3, the concentration of H_2O_2 5 mM and pH 8.0 was chosen as optimal conditions and the detailed information was shown in Supplementary materials (Fig. S8). Under the optimized conditions, the ECL intensity decreased with the increase of Aβ proteins' concentrations in Fig. 4A (curve a-i). As shown in Fig. 4B, a linear relationship between ECL response of the developed immunosensor and the logarithm of Aβ proteins' concentrations was obtained from 0.05 pg mL^{-1} to 10 ng mL^{-1}. The linear equation was I = -1006.3 Log c + 1195.2, with a correlation coefficient of 0.9862 and a detection limit of 21 fg mL^{-1} (S/N = 3). It is worth to note that the proposed immunosensor in our work represented satisfied linear range and limit of detection (Table S2) compared with previous developed immunosensor, indicating its excellent performance in Aβ proteins analysis.

3.5. Stability, specificity and reproducibility of the constructed ECL immunosensor

The stability of the synthesized luminophore materials and the fabricated immunosensor was one of the major concerns for practical applications. As shown in Fig. S9, Luminol-Au@MoS_2/Bi_2S_3 composites exhibited excellent ECL stability with the relative standard deviation (RSD) of 0.93%. When the concentration of Aβ proteins was 0.1 ng mL^{-1}, the immunosensor was conducted in PBS (pH = 8.0) with 5 mM H_2O_2 under 15 cycles of continuous potential scans. According to Fig. 4C, RSD was 1.2%, indicating that the developed immunosensor showed satisfied results.

In order to assess the specificity of the prepared ECL immunosensor, interferences study was carried out using alpha-fetoprotein (AFP) and carcinoembryonic antigen (CEA) as an example. As shown in Fig. 4D, when the antigen was blank, AFP and CEA, these three ECL signals were no obvious difference and quite high. But when the analytes containing Aβ proteins (0.1 ng mL^{-1}), ECL signal was no obvious change between

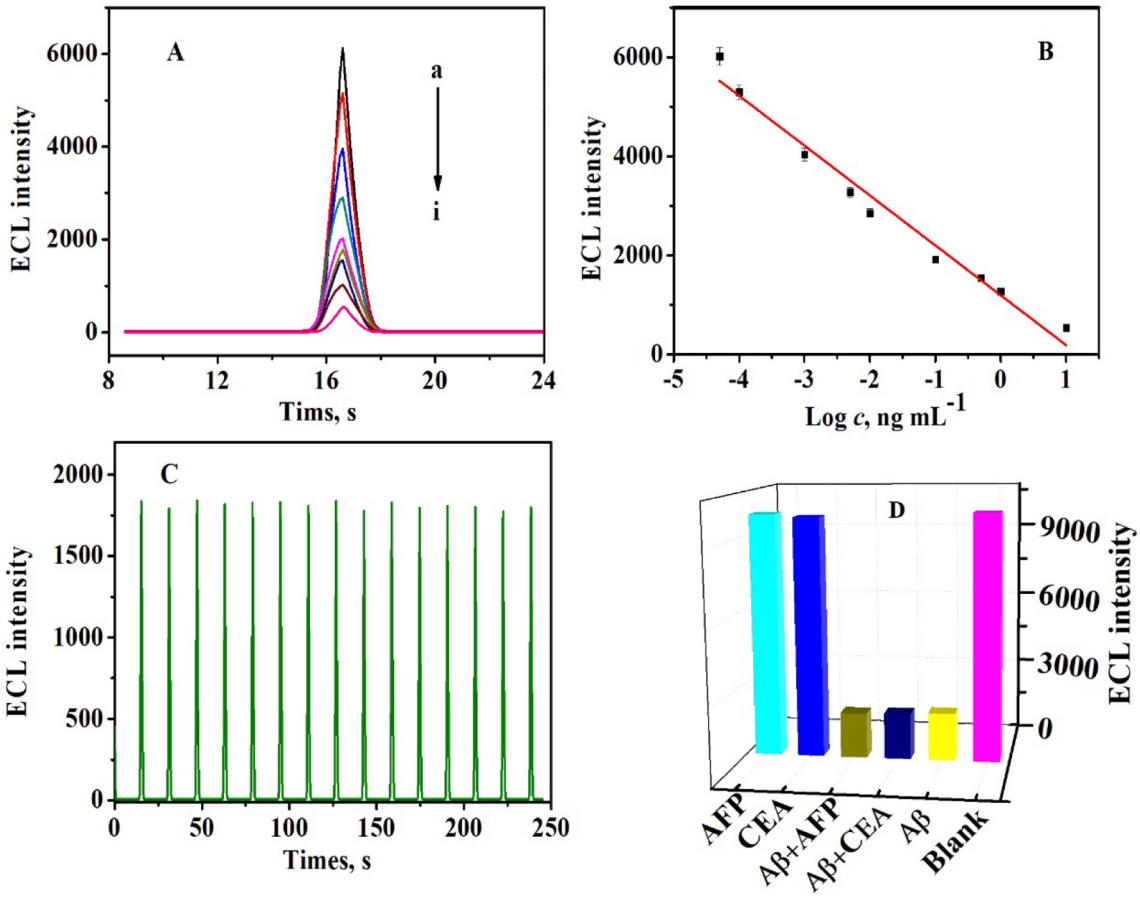

Fig. 4. (A) ECL response of the immunosensor towards different concentrations of Aβ proteins, from a to i: 5E-5, 1E-4, 1E-3, 0.005, 0.01, 0.1, 0.5, 1 and 10 ng mL^{-1}. (B) The relationship between the concentration of Aβ proteins and ECL intensities. (C) Stability of ECL emissions under continuous scanning for 15 cycles in PBS (pH = 8.0) containing 5 mM H_2O_2 for detection of 0.1 ng mL^{-1} Aβ proteins. (D) Selectivity of the proposed ECL immunosensor: blank, AFP (10 ng mL^{-1}), CEA (10 ng mL^{-1}), Aβ proteins (0.1 ng mL^{-1}), and the mixture (containing 10 ng mL^{-1} of AFP, 10 ng mL^{-1} of CEA, and 0.1 ng mL^{-1} of Aβ proteins). Error bars = RSD (n = 3).

Table 1
Analytical application of the immunosensor in artificial cerebrospinal fluid.

Sample	Addition (ng mL^{-1})	Found (ng mL^{-1})	Recovery (%)
1	1	1.12	112
2	0.1	0.109	109
3	0.05	0.047	94
4	0.001	0.00104	104

pure Aβ proteins and a mixed solution (including 0.1 ng mL^{-1} Aβ proteins, 10 ng mL^{-1} AFP and 10 ng mL^{-1} CEA), indicating that the developed immunosensor exhibited excellent specificity.

The reproducibility of the ECL immunosensor was discussed through fabricating six same electrodes. The RSD was 1.04% and 3.63% for analyzing 0.05 pg mL^{-1} and 10 ng mL^{-1} Aβ proteins (Fig. S10), indicating the satisfying reproducibility of the immunosensor. In addition, the ECL response of the as-prepared immunosensor decreased 5.6% after 10-day storage at 4 °C. The results indicated that the immunosensor had satisfying stability both in a long time.

3.6. Application of the prepared ECL Immunosensor in artificial cerebrospinal fluid

To investigate the potential of the ECL immunosensor in AD detection, the immunosensor was carried out to detect the recovery of different Aβ proteins' concentrations in artificial cerebrospinal fluid by standard addition method. From the Table 1, the recovery of Aβ proteins was in the range of 94–112%. The results indicated that the developed immunosensor held promising potential for the analyzation of Aβ proteins in artificial cerebrospinal fluid.

4. Conclusion

In summary, the ECL immunosensor with curcumin as an effective quencher for luminol/H_2O_2 system was developed for detecting Aβ proteins. Luminol-Au@MoS_2/Bi_2S_3 composites have exhibited excellent ECL behavior due to MoS_2/Bi_2S_3 nanorods anchored more Au nanoparticles through Au-S binding for plenty of luminol-Au complexes loading. The hydrophobic curcumin was successfully doped in ZnO materials which can effectively quench the ECL behavior of luminol and PDA can wrap the surface of ZnO-CR binding with Ab_2. The possible quenching mechanism may be due to energy transfer and the consumption of and $O_2^{\cdot-}$ produced by coreactant H_2O_2. The fabricated immunosensor exhibited excellent performances of stability, accuracy and reproducibility. Moreover, this work may broaden the application of curcumin for detecting other targets, but the hydrophobicity of curcumin may limit its application in bioanalysis.

CRediT authorship contribution statement

Xiaojian Li: Conceptualization, Data curation, Writing - original draft. **Dan Wu:** Formal analysis. **Hongmin Ma:** Methodology, Writing - review & editing. **Huan Wang:** Methodology. **Yaoguang Wang:** Investigation. **Dawei Fan:** Formal analysis. **Bin Du:** Funding acquisition, Project administration. **Qin Wei:** Funding acquisition, Project administration. **Nuo Zhang:** Methodology, Writing - review & editing.

Acknowledgements

This study was supported by the National Key Scientific Instrument and Equipment Development Project of China (No. 21627809), National Natural Science Foundation of China (Nos. 21575050, 21505051 and 21777056), the Technology Research Project of Shandong Provincial Education Department (No. J15LC07) and the Special Foundation for Taishan Scholar Professorship of Shandong Province (No. ts20130937) and UJN.

Declaration of interests

The authors declare that they have no known competing financial interests or personal relationships that could have appeared to influence the work reported in this paper.

Appendix A. Supporting information

Supplementary data associated with this article can be found in the online version at https://doi.org/10.1016/j.bios.2019.01.066.

References

Ahmed, K., Li, Y., Mcclements, D.J., Xiao, H., 2012. Food Chem. 132 (2), 799–807.
Anand, P., Thomas, S.G., Kunnumakkara, A.B., Sundaram, C., Harikumar, K.B., Sung, B., Tharakan, S.T., Misra, K., Priyadarsini, I.K., Rajasekharan, K.N., 2008. Biochem. Pharmacol. 76 (11), 1590–1611.
Chen, Y., Zhao, S., Chen, M., Zhang, W., Mao, J., Zhao, Y., Maitz, M.F., Huang, N., Wan, G., 2015. Corros. Sci. 96, 67–73.
Christian, S., Margareth, P., Maike, P., Volker, S., Donat, K., Jakob, W., 2010. Bmc Cancer 10 (1), 491–498.
Ciszewski, A., Milczarek, G., Lewandowska, B., Krutowski, K., 2003. Electroanalysis 15 (5–6), 518–523.
El, K.E., Abiad, M., Kassaify, Z.G., Patra, D., 2015. Colloids Surf. B Biointerfaces 127, 274–280.
Fang, L., Qiu, Y., Zhai, T., Wang, F., Lan, M., Huang, K., Jing, Q., 2017. Colloids Surf. A: Physicochem. Eng. Asp. 535, 41–48.
Fang, L., Zhang, B., Li, W., Zhang, J., Huang, K., Zhang, Q., 2014. Electrochim. Acta 148, 164–169.
Gangwar, R.K., Tomar, G.B., Dhumale, V.A., Zinjarde, S., Sharma, R.B., Datar, S., 2013. J. Agric. Food Chem. 61 (40), 9632–9637.
Govindaraju, S., Rengaraj, A., Arivazhagan, R., Huh, Y.S., Yun, K., 2018. Bioconjugate Chem. 29 (2), 363–370.
Han, Q., Wang, R., Xing, B., Zhang, T., Khan, M.S., Wu, D., Wei, Q., 2017. Biosens. Bioelectron. 99, 493–499.
Hatcher, H., Planalp, R., Cho, J., Torti, F.M., Torti, S.V., 2008. Cell. Mol. Life Sci. 65 (11), 1631–1652.
Hong, X., Kim, J., Shi, S.F., Zhang, Y., Jin, C., Sun, Y., Tongay, S., Wu, J., Zhang, Y., Wang, F., 2014. Nat. Nanotechnol. 9 (9), 682–686.
Jiang, X., Wang, Z., Wang, H., Zhuo, Y., Yuan, R., Chai, Y., 2017. Chem. Commun. 9705–9708.
Khalil, M.I., Al-Zahem, A.M., Qunaibit, M.M., 2013. Med. Chem. Res. 23 (23), 1683–1689.
Kim, J.H., Lee, M., Park, C.B., 2014. Angew. Chem. Int. Ed. Engl. 53 (25), 6364–6368.
Kolev, T.M., Velcheva, E.A., Stamboliyska, B.A., Spiteller, M., 2005. Int. J. Quantum Chem. 102 (6), 1069–1079.
Li, X., Yu, S., Yan, T., Zhang, Y., Du, B., Wu, D., Wei, Q., 2017. Biosens. Bioelectron. 89, 1020–1025.
Liu, L., Sun, L., Wu, Q., Guo, W., Li, L., Chen, Y., Li, Y., Gong, C., Qian, Z., Wei, Y., 2013. Int. J. Pharm. 443 (1–2), 175–182.
Liu, X., Jiang, H., Lei, J., Ju, H., 2007. Anal. Chem. 79 (21), 8055–8060.
Liu, X., Zhang, G., Zhang, Y.W., 2016. Nano Res. 9 (8), 2372–2383.
Moussawi, R.N., Patra, D., 2015. J. Phys. Chem. C 119 (33), 19458–19468.
Moussawi, R.N., Patra, D., 2016. Rsc Adv. 6 (21), 17256–17268.
Pan, K., Zhong, Q., Baek, S.J., 2013. J. Agric. Food Chem. 61 (25), 6036–6043.
Patil, P.B., Parit, S.B., Waifalkar, P.P., Patil, S.P., Dongale, T.D., Sahoo, S.C., Kollu, P., Nimbalkar, M.S., Patil, P.S., Chougale, A.D., 2018. Mater. Lett. 223, 178–181.
S, M., M, C., C, Z., D, A., A, N., B, L.F., M, S., F, N., M, G., SG, A., 2011. Biomaterials 32 (6), 1635–1645.
Selkoe, D.J., 2001. Physiol. Rev. 81 (2), 741–766.
Shankar, G.M., Bloodgood, B.L., Townsend, M., Walsh, D.M., Selkoe, D.J., Sabatini, B.L., 2007. J. Neurosci. 27 (11), 2866–2875.
Tapal, A., Tiku, P.K., 2012. Food Chem. 130 (4), 960–965.
Tikekar, R.V., Pan, Y., Nitin, N., 2013. Food Res. Int. 51 (1), 370–377.
Triguero, L., Singh, R., Prabhakar, R., 2008. J. Phys. Chem. B 112 (23), 7123–7131.
Vestergaard, M., Kerman, K., Saito, M., Nagatani, N., Takamura, Y., Tamiya, E., 2005. J. Am. Chem. Soc. 127 (34), 11892–11893.
Wang, R., Ma, H., Zhang, Y., Wang, Q., Yang, Z., Du, B., Wu, D., Wei, Q., 2017. Biosens. Bioelectron. 96, 345–350.
Yang, D.P., Guo, W., Cai, Z., Chen, Y., He, X., Huang, C., Zhuang, J., Jia, N., 2018. Sens. Actuators B Chem. 260, 642–649.
Yin, W., Yu, J., Lv, F., Yan, L., Zheng, L.R., Gu, Z., Zhao, Y., 2016. Acs Nano 10 (12), 11000–11011.
Yu, Y., Zhang, L., Li, C., Sun, X., Tang, D., Shi, G., 2014. Angew. Chem. 53 (47), 12832–12835.
Zhou, N., Zan, X., Wang, Z., Wu, H., Yin, D., Liao, C., Wan, Y., 2013. Carbohydr. Polym. 94 (1), 420–429.